Nanoscale

RSC Publishing

PAPER

View Article Online
View Journal

Direct observation of a single nanoparticle–ubiquitin corona formation†

Cite this: DOI: 10.1039/c3nr02147e

Feng Ding,*[ab] Slaven Radic,[a] Ran Chen,[a] Pengyu Chen,[a] Nicholas K. Geitner,[a] Jared M. Brown[c] and Pu Chun Ke*[a]

Received 29th April 2013
Accepted 10th July 2013

DOI: 10.1039/c3nr02147e

www.rsc.org/nanoscale

The advancement of nanomedicine and the increasing applications of nanoparticles in consumer products have led to administered biological exposure and unintentional environmental accumulation of nanoparticles, causing concerns over the biocompatibility and sustainability of nanotechnology. Upon entering physiological environments, nanoparticles readily assume the form of a nanoparticle–protein corona that dictates their biological identity. Consequently, understanding the structure and dynamics of a nanoparticle–protein corona is essential for predicting the fate, transport, and toxicity of nanomaterials in living systems and for enabling the vast applications of nanomedicine. Here we combined multiscale molecular dynamics simulations and complementary experiments to characterize the silver nanoparticle–ubiquitin corona formation. Notably, ubiquitins competed with citrates for the nanoparticle surface, governed by specific electrostatic interactions. Under a high protein/nanoparticle stoichiometry, ubiquitins formed a multi-layer corona on the particle surface. The binding exhibited an unusual stretched-exponential behavior, suggesting a rich binding kinetics. Furthermore, the binding destabilized the α-helices while increasing the β-sheet content of the proteins. This study revealed the atomic and molecular details of the structural and dynamic characteristics of nanoparticle–protein corona formation.

1 Introduction

Nanomaterials have been increasingly applied in consumer products due to their unique physical and chemical properties. The increasing application of nanomaterials in daily life inevitably leads to their accumulation in the environment[1] and subsequent entry into biological systems, causing bio-safety concerns related to nanotechnology.[2] Nanoparticles have also been found useful in disease diagnostics, drug delivery, and therapeutics.[3–5] Therefore, the safety issue of nanotechnology is pressing, and the study of nanotoxicology has attracted much research interest recently.[6] The benefits of understanding the interactions between nanoparticles and biological systems extend from fundamental physical sciences to nanomedicine, nanotoxicology, nanoecotoxicology, consumer usages, and the public's perception of nanotechnology.

Upon entering biological systems such as the bloodstream, a nanoparticle forms molecular complexes with encountered proteins, termed as the protein corona.[7] The protein corona shields the surface of the exogenous nanoparticle and subsequently determines the biological properties of the nanoparticle core.[8,9] Recently, the protein corona has been found to screen functionalized molecules conjugated with nanoparticles, and subsequently cause the loss of designed function.[10] In addition, interactions with nanoparticles can also alter the structure, dynamics, and function of the bound proteins, which could further impact recognition of the proteins by membrane receptors and the immune system. Previous experimental studies have provided much insight, such as the existence and size of the protein corona,[11] and protein composition on the nanoparticle surface.[12] However, due to limitations in the instrument resolution, the molecular details of the protein–nanoparticle interaction remain poorly understood. Computational modeling, in contrast, provides a useful approach to bridge the gap between experimental observations and the molecular systems of interest.[13] Here we performed both computational and experimental characterization of protein corona formation between a silver nanoparticle (AgNP) and ubiquitin protein. Silver nanoparticles are widely used in commercial products for their antibacterial and antifungal properties,[14] while ubiquitin is ubiquitously expressed in all eukaryotic cells regulating protein distribution and recycling,

[a]Department of Physics and Astronomy, COMSET, Clemson University, Clemson, SC 29634, USA. E-mail: fding@clemson.edu; pcke11@clemson.edu

[b]Department of Biochemistry and Biophysics, School of Medicine, University of North Carolina at Chapel Hill, Chapel Hill, NC 27599, USA

[c]Department of Pharmaceutical Sciences, Skaggs School of Pharmacy, The University of Colorado Anschutz Medical Campus, Aurora, CO 80045, USA

† Electronic supplementary information (ESI) available: Experimental and computational methods as well as supporting figures. See DOI: 10.1039/c3nr02147e

thereby making AgNP and ubiquitin a representative model system for studying the nanoparticle–protein interaction and corona formation.

Two major challenges arise in computational modeling of a protein corona. First is the large system size, where an abundance of proteins interacts with nanometer-sized nanoparticles, and second is the long timescales associated with protein corona formation. Traditional molecular dynamics approaches can accurately describe the molecular system of nanoparticles and proteins,[15–18] but are not able to reach the relevant time and length scales needed for depicting large systems till equilibration.[19,20] In comparison, coarse-grained simulations[21] can be used to study large molecular systems and reach long time scales by using a simplified force field.[22] These coarse-grained simulations have been applied to study general aspects of NP–protein interactions,[21,23–26] but have limited predictive power for studying NP interactions with specific proteins. To overcome this barrier, we adopted a multiscale modeling approach,[27] which coherently blended atomistic and coarse-grained simulations.[28,29] All-atom simulations were first performed to investigate the possible binding modes between an individual ubiquitin and a AgNP, and the knowledge of AgNP–ubiquitin binding was then incorporated into the construction of a coarse-grained model. With the coarse-grained simulations, we were able to extensively characterise the structure and dynamics of AgNP interacting with multiple ubiquitin molecules (up to 50). The dynamics of both atomistic and coarse-grained models were sampled by discrete molecular dynamics (DMD),[30] an efficient sampling method for underpinning protein dynamics (ESI†).

2 Results and discussion

Our transmission electron microscopy (TEM) and UV-vis absorbance measurements (Experimental section, ESI†) confirmed the binding of ubiquitin and citrate-coated AgNP (Fig. 1A and B). For UV-vis, specifically, a red-shift occurred from 393 nm (peak wavelength for AgNP absorbance) to 407 nm (peak wavelength for AgNP–ubiquitin absorbance), indicating an increased dielectric constant resulting from nanoparticle–protein complex formation. Consistently, our dynamic light scattering measurements (ESI, Fig. S1†) showed a hydrodynamic size of 34.5 nm for AgNP–ubiquitin at molar ratios of 1 : 100 to 1 : 500 (zeta potential: 12.3 mV), compared to that of 4.8 nm for ubiquitins (zeta potential: 4.6 mV) and 13.6 nm for AgNPs (zeta potential: −45.0 mV) alone, further corroborating their effective binding.

Next, we performed multiscale simulations to characterize the nanoparticle–ubiquitin corona formation *in silico*. We first performed atomistic simulations of a molecular system comprised of one ubiquitin molecule and one citrate-coated AgNP (ESI†). The simulations were performed with an implicit solvent, and the inter-atomic interactions were modeled by a physical force field adapted from Medusa,[31] which include van der Waals, solvation,[32] electrostatic, and hydrogen bond potentials. We developed a simplified AgNP model (ESI†), where the model parameters were assigned to capture the general properties of the molecular system instead of reproducing every aspect of molecular details. For instance, the coarse-grained silver atoms of the AgNP were assigned as hydrophobic with a small fraction being positively charged to account for the residual silver ions on the nanoparticle surface. We included excessive citrate molecules in simulations to model the experimentally observed negative zeta-potential of the citrate-capped AgNP.[33] During simulations, we kept the center of the AgNP static, while allowing the ubiquitin and the citrates to move freely in the simulation box and surface silver atoms mobile on the NP surface. Since the physical properties of the coarse-grained AgNP model are rather general, the observed behaviors of AgNP–ubiquitin binding should be readily applicable to other metallic nanoparticles with positive surface charges, such as gold nanoparticles (AuNPs).

To evaluate whether ubiquitin could bind to a citrate-coated AgNP, we performed DMD simulations at 300 K with a ubiquitin molecule initially positioned away from a citrate-coated AgNP (Fig. 1C). Interestingly, we found that the neutral ubiquitin did not bind to the hydrophobic surface of the AgNP, but instead attracted to the surface charge of the AgNP by replacing the surface-bound citrates ($-3e$ at neutral pH) that were stabilized by electrostatic interactions (Fig. 1C). Although ubiquitin does not have a net charge, it does possess eleven positively charged and eleven negatively charged residues out of the 76 total residues.[34] Near the surface of the ubiquitin helix, negatively charged residues formed a cluster with low electrostatic potentials (Fig. 1D), which favored the electrostatic interaction with counter charges.[35] The local surface area with low electrostatic potential allowed a stronger binding to the AgNP in simulations than did the negatively charged citrates.

To test whether the electrostatic interaction was the driving force for AgNP–ubiquitin binding, we artificially enhanced the binding affinity between citrates and AgNP by adding an additional charge to the citrate molecule (ESI†). For both the case of artificially enhanced electrostatic interactions and the regular (non-enhanced) case, we performed ten independent atomistic DMD simulations with different initial AgNP/ubiquitin configurations, including different relative orientations, intermolecule distances, and velocities. For a higher citrate–AgNP affinity due to enhanced electrostatic interactions, we did not observe any AgNP–ubiquitin binding in all simulations. In the case of regular citrate–AgNP interactions, we observed AgNP–ubiquitin binding for seven out of ten simulations. The computed distributions of citrates from the AgNP also illustrated that the ability of ubiquitin to displace citrates and bind AgNP depended upon the electrostatic-dominating affinity between the citrates and the AgNP (Fig. 1E). Therefore, the binding of ubiquitin to AgNP was mainly determined by electrostatic interactions.

For independent atomistic simulations with different initial configurations, we found that ubiquitins formed similar bound structures with AgNP. From these simulations, we constructed a structural ensemble of the AgNP–ubiquitin binding complex. We averaged over the ensemble to compute for each residue the probability of forming contact with the AgNP, P_{AgNP}, (ESI†). Only a subset of protein residues showed significantly high contact

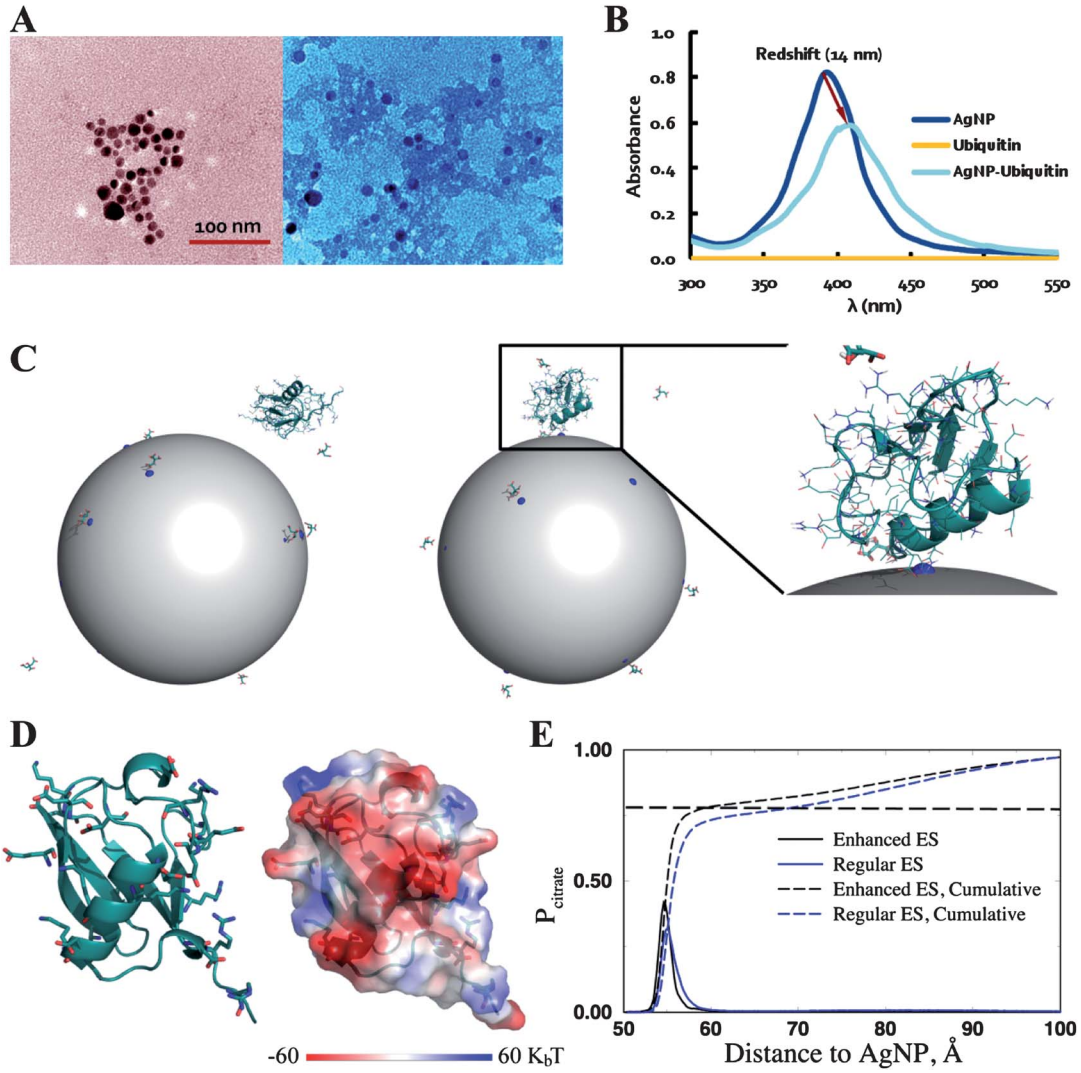

Fig. 1 Interaction between a single ubiquitin and a citrate-coated AgNP. (A) TEM images of AgNPs (left panel) and AgNP–ubiquitin coronas (right panel) where the associations of the AgNPs and the proteins (shaded regions) are evident to imply their good binding affinity. (B) UV-vis absorbance of AgNP, ubiquitin, and AgNP–ubiquitin, featuring a red-shift of the absorbance peaks for AgNP–ubiquitin and AgNP alone due to dampened surface plasmon resonance. (C) Initial ($t = 0$ ns) and final ($t = 50$ ns) structure of the ubiquitin–citrate–AgNP complex system. Ubiquitin is represented as cartoons, the side chains as lines, and the citrates as sticks. The gray sphere represents the nanoparticle, and the charged atoms on the AgNP surface are shown as blue spheres. The zoom-in view of the final structure indicates the binding between the ubiquitin and a charged AgNP surface atom. (D) The negatively (aspartate and glutamate) and positively (lysine and arginine) charged residues in ubiquitin are shown as sticks (left panel). The surface electrostatic potential (computed using PyMol, http://www.pymol.org) illustrates the cluster of negatively charged atoms near the protein helix (right panel). (E) Distribution of citrates around AgNP (solid lines) derived from the simulations. The electrostatic (ES) interaction between citrate and AgNP was artificially enhanced in one case. The dashed lines correspond to the accumulative probability. The horizontal dashed line corresponds to charge saturation, where the total charge of citrates is equal to that of the AgNP.

frequencies, while the rest of the protein did not interact with the AgNP (Fig. 2A). As the result, the histogram of P_{AgNP} featured a bimodal distribution, with one peak close to zero and the other centered around $P_{AgNP} \sim 0.4$ (Fig. 2B). We further determined the AgNP-binding residues (Fig. 2B, inset) as those with P_{AgNP} larger than 0.3, the median value separating two peaks in the histogram. These residues were located near the protein helix (Fig. 1D). Although the electrostatic interaction was identified as the driving force for AgNP–ubiquitin binding, intriguingly only a fraction of the negatively charged residues had high contact frequencies with the positively charged AgNP surface (Fig. 2A). Since these negatively charged residues are scattered on the surface of ubiquitin (Fig. 1C), it was unknown *a priori* where these AgNP-binding residues were located. Next, we compared our results with a nuclear magnetic resonance (NMR) study of ubiquitin–gold nanoparticle (AuNP) binding.[36] In the NMR study, the chemical shift of backbone NH groups was monitored upon ubiquitin binding to the AuNP. Since the NMR chemical shift is very sensitive to the corresponding environment, chemical shift perturbations could be caused either by direct binding with the AuNP or due to NP-binding induced conformational changes. Three residues—2, 15, and 18—were found to have significant chemical shift perturbations upon binding to the AuNP. These residues are close to each

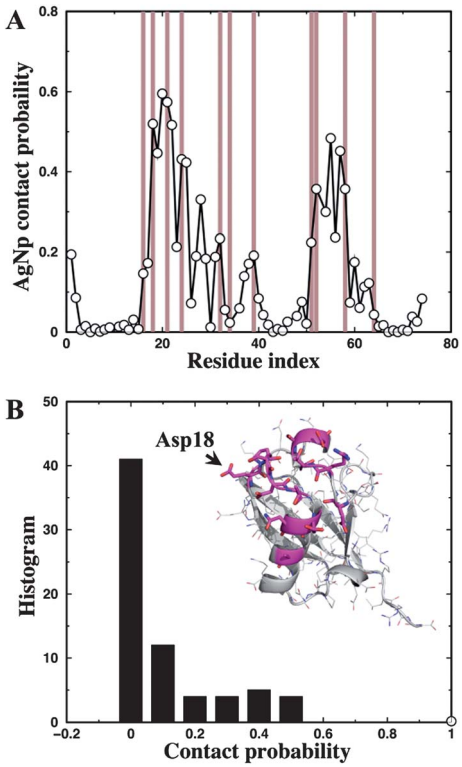

Fig. 2 Specific binding between ubiquitin and AgNP. (A) The contact probability between AgNP and each ubiquitin residue, computed from independent all-atom DMD simulations (ESI†). The shaded regions correspond to negatively charged residues, including both aspartate (Asp) and glutamate (Glu). (B) The histogram of the AgNP–ubiquitin contact probability displays a bimodal distribution. The ubiquitin residues with high contact frequency (>0.3; corresponding to the second peak) to the AgNP are shown in sticks (inset). The residue Asp18 was also found to interact with gold nanoparticles.[36]

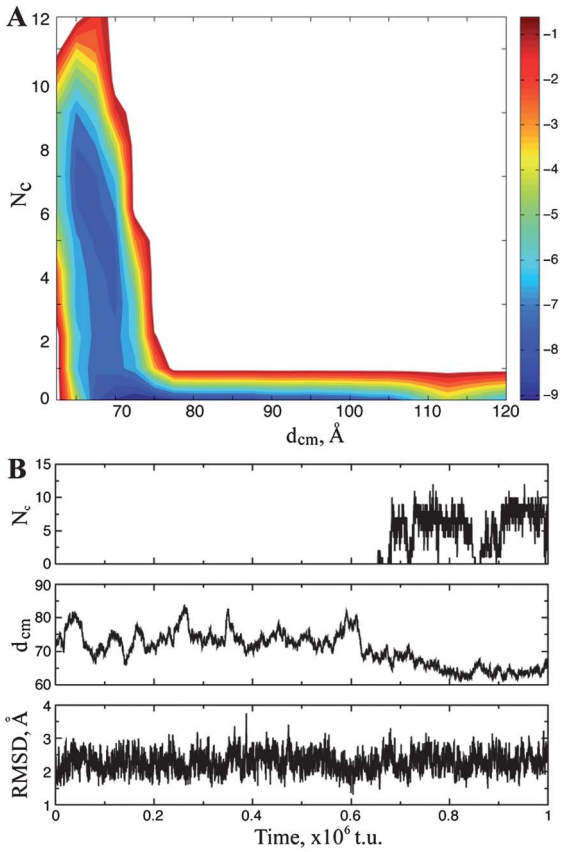

Fig. 3 AgNP–ubiquitin binding thermodynamics. (A) Contour plot of the 2D-PMF with respect to the inter-molecule distance, d_{cm}, and the number of specific inter-molecule contacts, N_c. The unit of PMF is kcal mol^{-1}. (B) A typical trajectory of the all-atom simulation of AgNP–ubiquitin binding. N_c, d_{cm}, and the RMSD of ubiquitin are shown as functions of the simulation time, in DMD time unit (t.u., ESI†).

other in the 3D structure, suggesting the corresponding surface area bound to the AuNP. In our simulations, the residue 18 had a high contact frequency with the AgNP and the residue 2 also formed contact with AgNP (Fig. 2A). The reason that we did not observe the residue 15 in contact with the AgNP is due to the fact that leucine 15 is buried inside the protein. Since AgNP and AuNP are comparable both physically and chemically, we believe that the modes of their binding with ubiquitin are also comparable. This agreement between NMR observations and simulations highlights the predictive power of our computational methods.

We further investigated the thermodynamics of AgNP–ubiquitin binding by computing the potential of mean force, PMF (ESI†). We calculated the 2D-PMF with respect to the centre-of-mass distance between AgNP and ubiquitin, d_{cm}, and the number of contacts between AgNP and the residues identified to bind AgNP specifically, N_c (Fig. 3A). The 2D-PMF plot has two minima. One minimum corresponds to non-specific binding, where $N_c = 0$ and $d_{cm} \sim 70$ Å, while the other one represents the specific binding with $N_c > 0$ and $d_{cm} < 70$ Å. The barrier separating two minima corresponds to the re-orientation of the protein as illustrated in a typical simulation trajectory (Fig. 3B). Before specific binding ($t < 0.7 \times 10^6$ t.u.), the system featured a large fluctuation of d_{cm} with the protein near the AgNP surface ($d_{cm} \sim 70$ Å). The protein had similar root-mean-square deviation (RMSD) from its native state before and after specific binding to AgNP. Therefore, protein re-orientation on the surface of AgNP was the rate-limiting step toward the specific binding.

In order to observe the formation of AgNP–ubiquitin corona *in silico*, it is necessary to include multiple proteins in simulations, which is beyond the capacity of atomistic simulations. Instead, we used a two-bead-per-residue model[37] to represent ubiquitin and a single atom to model each citrate. The inter- and intra-ubiquitin interactions were modeled by a structure-based potential model,[38,39] which has been extensively used in computational studies of protein folding and protein aggregation.[29] The specific interactions between the AgNP surface charges and ubiquitin residues as well as other non-specific inter-molecule interactions were modeled according to atomistic DMD simulations (ESI†).

We investigated AgNP–ubiquitin corona formation by performing DMD simulations of the coarse-grained system, with multiple ubiquitins (25 molecules) initially positioned randomly with respect to a citrate-coated AgNP. The

temperature of the simulation system was maintained at 325 K, which is below the melting temperature of ubiquitin, $T_m = 340$ K (ESI, Fig. S2†). Therefore, an isolated protein was thermodynamically stable, mimicking the physiological conditions where the protein remains folded. To avoid potential biases associated with initial conditions, we performed ten independent simulations assuming different initial configurations and velocities. For each simulation we monitored the number of ubiquitins directly bound to the surface of AgNP, N_{bound}, as a function of time. All trajectories in Fig. 4A featured an initial fast binding, which slowed down as time progressed. Interestingly, the average N_{bound} did not follow a typical single-exponential binding kinetics, $\sim 1 - \exp(-\lambda t)$, which usually features a power-law with the exponent of 1 during initial binding in a log–log plot (Fig. 4B). Instead, the exponent is $\sim 0.21 < 1$. Fitting analysis (ESI†) suggested that a stretched-exponential, $\sim 1 - \exp(-ct^{\alpha})$, better represented the kinetics data. Similar stretched-exponential binding kinetics has been reported for the adsorption of human serum albumin on a colloidal nanoparticle.[40] A stretched exponential function, corresponding to a linear superposition of exponential decays with a continuous distribution of relaxation times, is often used

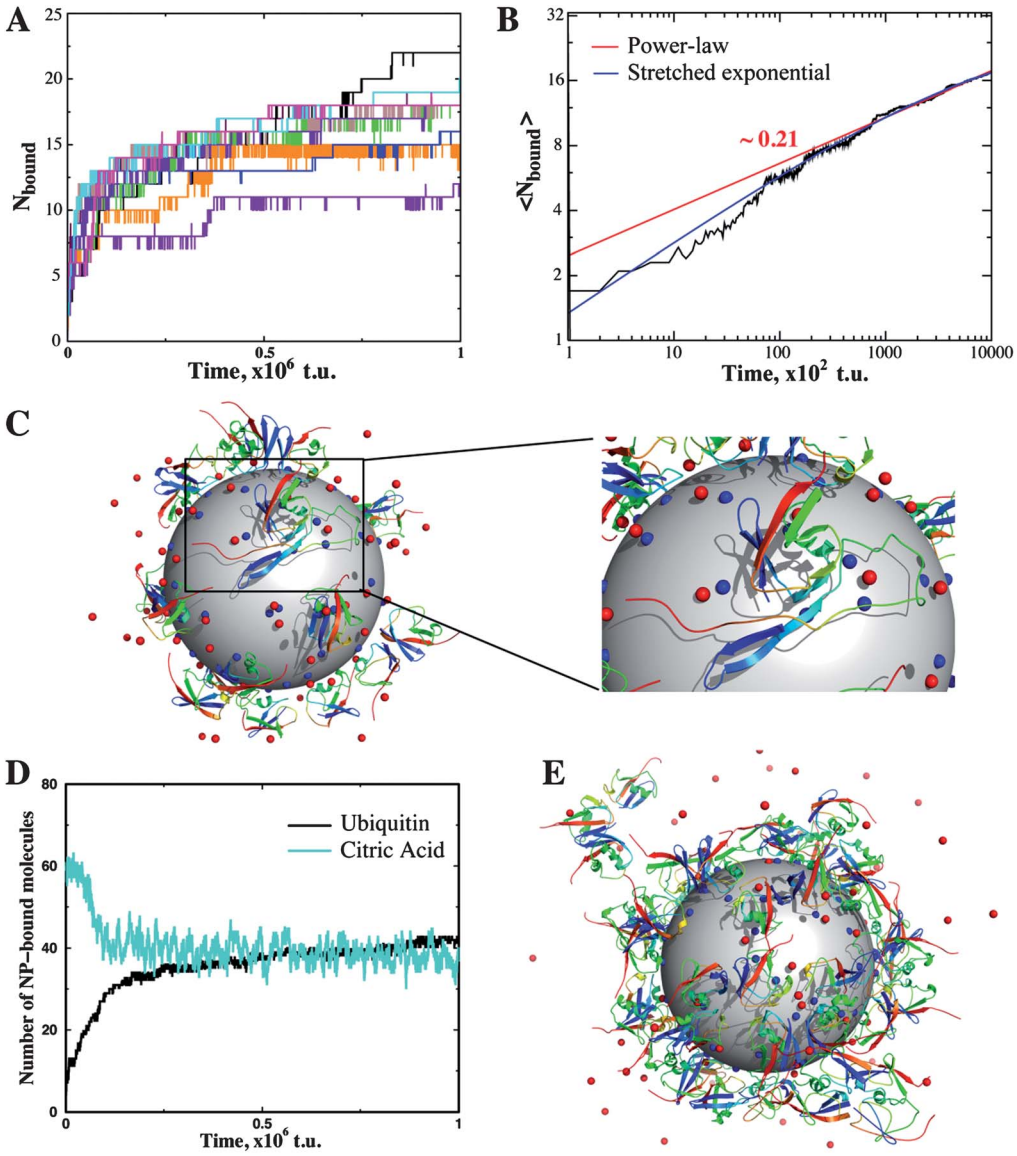

Fig. 4 Ubiquitin–AgNP corona formation. (A) The number of ubiquitin molecules bound to AgNP, N_{bound}, was computed as the function of time (in DMD time unit, t.u., see ESI†) from ten independent simulations (in different colors) of the coarse-grained molecular system. (B) The average number of ubiquitins bound to AgNP, $\langle N_{bound} \rangle$, features a power-law (approximately linear) in a log–log plot. A power-law fit has an exponent of 0.21. A stretched exponential, $\sim 1 - \exp(-ct^{\alpha})$, better fits the data with $\alpha = 0.34$. (C) The final structure from one of the simulations (corresponding to the black line with the highest N_{bound} in panel (A)). The ubiquitins are represented as cartoons. The citrates correspond to the red spheres. The large gray sphere denotes the AgNP, and the blue spheres on the surface of the AgNP are the positively charged atoms. One of the AgNP-bound ubiquitin is unfolded on the nanoparticle surface (right). In a coarse-grained DMD simulation with a higher stoichiometry of ubiquitin to AgNP (50 : 1), ubiquitin (black line) competed with citrate (red) to bind AgNP by displacing initially bound citrates (D). At this high stoichiometry, multi-layers of ubiquitins were found to deposit onto the surface of the AgNP (E).

to describe the relaxation kinetics with high heterogeneity in the relaxation time. The heterogeneity could originate from competition with citrates, depletion of available binding sites for incoming ubiquitins, and non-specific interactions with other proteins. The binding rate between citrate and AgNP was concentration-dependent, and increased as ubiquitins displaced AgNP-bound citrates and subsequently increased the citrate concentration in solution. Examination of the simulation trajectories also suggested non-specific binding between the incoming protein and the proteins already bound to the surface, which slowed down the specific binding with NP (Fig. S3†). All these factors hindered the binding of ubiquitins to the AgNP surface, leading to the stretched exponential binding kinetics.

A stretched exponential decay of the protein concentration in solution, $[\mathrm{p}] \sim \exp(-ct^{\alpha})$ with $\alpha < 1$, suggests that the association rate $-(\mathrm{d}[\mathrm{p}]/\mathrm{d}t)/[\mathrm{p}] \sim 1/t^{1-\alpha}$ decreased as the time increased and as more proteins bound to the NP surface. Assuming that the dissociation rates were the same for all proteins, the binding constant decreased as more proteins bound to the NP surface, which is indicative of the lack of binding cooperativity among the proteins. This observed anti-cooperativity is possibly a result of both steric hindrance[40] and non-specific protein–protein interactions (Fig. S3†). Therefore, our coarse-grained simulations revealed a rich kinetics for nanoparticle–protein binding, which may need to be considered in future kinetic and mesoscopic modeling of corona formation, such as studies of the Vroman effect of abundant proteins for a nanoparticle entering the bloodstream.[41]

The AgNP–ubiquitin complex structure derived from simulations had multiple ubiquitins bound to the surface of one AgNP, forming a single-layer protein corona (Fig. 4C). The majority of AgNP-bound proteins stayed folded under the particular simulation condition (ESI†) and bound to the surface of the AgNP with the protein helix facing the nanoparticle. Only in one of the simulations, one ubiquitin out of the 22 AgNP-bound proteins partially unfolded and the conformation was stabilized by extensive contact with the hydrophobic surface of the AgNP (Fig. 4C). In addition, we explored the effect of protein concentration on the corona formation by performing DMD simulation for a higher ubiquitin/AgNP stoichiometry of 50 : 1. In these simulations, ubiquitins competed with citrates for binding to the AgNP (Fig. 4D). The final structure featured multiple layers of protein corona, whereas the first layer was dominated by specific binding between ubiquitins and the AgNP, and the outer layers were stabilized by protein–protein interactions (Fig. 4E). This observation is consistent with our dynamic light scattering measurement (Fig. S1†), where the hydrodynamic size of AgNP–ubiquitin increased from ~35 nm at AgNP : ubiquitin ratios of 1 : 100 and 1 : 500 to 44 nm and 52 nm at AgNP : ubiquitin ratios of 1 : 1000 and 1 : 2000, respectively. Hence, the AgNP–ubiquitin complex structures derived from the coarse-grained simulations successfully revealed an atomic picture of the nanoparticle–protein corona.

The ability of nanoparticles to induce protein unfolding in the corona (Fig. 4C) could be one of the mechanisms of

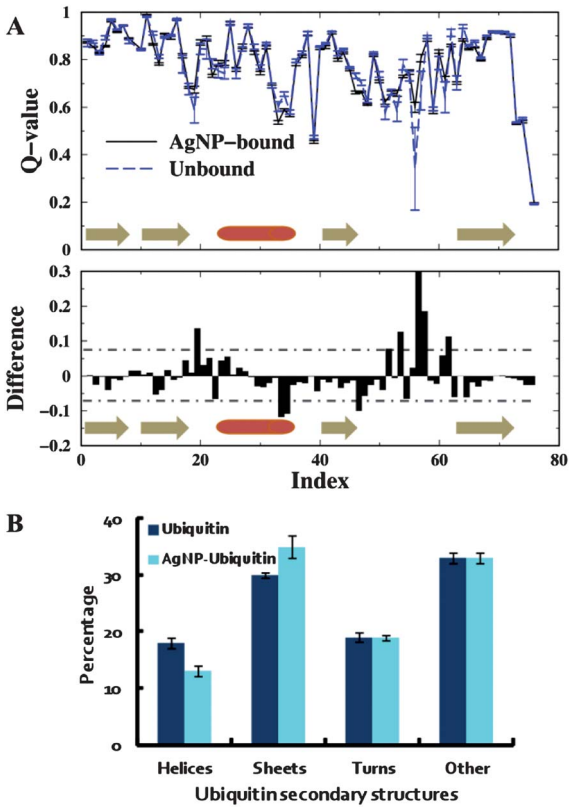

Fig. 5 The structural change of ubiquitin upon AgNP binding. (A) The fraction of native contacts, *Q*-value, was computed for each residue for both the AgNP-bound (black) and unbound (blue) ubiquitins (top panel). The error bars were estimated from independent simulations. The yellow arrows indicate the residue segments forming β-strands, and the red rod denotes the residues forming the α-helix. The differences of *Q*-value were computed between AgNP-bound and unbound (bottom panel) cases. The two dashed lines correspond to deviations with one standard deviation above and below the average. The differences beyond the two lines are statistically significant. (B) The percentage of secondary structures in ubiquitin (dark blue) and in AgNP–ubiquitin (cyan) was probed by CD experiments (ESI, Fig. S4†).

nanotoxicity. To evaluate the impact of AgNP-binding on the ubiquitin conformation, we computed for each protein residue the fraction of native contacts (*Q*-value[42]) for both the AgNP-bound and unbound ubiquitins (Fig. 5A). A residue with its *Q*-value close to 1 maintains a native-like structure, but loses its structure if the *Q*-value is near 0. Both the AgNP-bound and unbound ubiquitins maintained native-like structures with most regions having their *Q*-values close to 1. Only loop regions between the secondary structures (18–19, 32–35, and 46–53) had relatively low *Q*-values. The difference in the *Q*-values for AgNP-bound and unbound ubiquitins suggests that residues in contact with the AgNP were stabilized upon binding (the regions with positive differences coincided with the residues bound to AgNP, Fig. 2A). Two regions, one near the C-terminal of the helix and the other close to the residue 46 in a loop, were significantly destabilized upon binding. The destabilization of the protein helix due to AgNP-binding is consistent with our circular dichroism (CD) measurement (ESI, Fig. S4†), which revealed that the helical content was reduced by 27.8% relatively for the AgNP-bound ubiquitins compared to the free ubiquitins

(Fig. 5B). Our CD experiment also revealed a small increase in the β-sheet content. Since the *Q*-value is computed based on the protein native structure, it cannot measure the gain of secondary structures beyond the native state. With the protein concentration locally enriched on the AgNP surface, the increase of β-sheet content could result from the formation of inter-protein hydrogen bonds between partially unfolded protein regions. The formation of inter-protein hydrogen bonds could further lead to protein aggregation,[43] which requires further investigation in future studies.

3 Conclusions

In summary, both our computer simulations and experiments showed that ubiquitin proteins could readily bind to a citrate-coated AgNP to render a multilayer nanoparticle–protein corona. Despite many negatively charged residues scattered on the ubiquitin surface, our multiscale modeling revealed a specific binding between ubiquitins and AgNP driven by electrostatic interactions. Notably, our coarse-grained simulations of AgNP–ubiquitin corona formation uncovered an unusual stretched exponential binding kinetics, in agreement with a recent fluorescence kinetics measurement of nanoparticle–human serum albumin corona formation.[40] At a high stoichiometry, specifically, ubiquitins formed a multi-layer corona surrounding the AgNP. Both our simulations and experiments showed that AgNP-binding moderately destabilized the α-helix while it increased the β-sheet content of the ubiquitins. Taken together, our new multiscale modeling method was able to recapitulate various structural and dynamic characteristics of the nanoparticle–protein corona observed experimentally, and offered an atomic detail and a mechanistic insight into nanoparticle–protein self-assembly. Since the topic of protein corona and, especially, the connections between nanoparticle–protein corona with the transformation, biocompatibility, and immune responses of nanoparticles are still poorly understood, we believe that our method will find broad implications and applications in the research areas of molecular self assembly, physical adsorption, nanobiophysics, nanomedicine, and the health and safety of nanotechnology.

4 Experimental and computational methods

We combined both experimental and computational approaches to characterize the formation of nanoparticle–ubiquitin corona. The details of both experimental and computational methods can be found in the ESI.†

Acknowledgements

The work was supported in part by the NSF Grant CBET-1232724 (to P.C.K.), an NIEHS grant R01 ES019311 02S1 (to J.M.B. and P.C.K.), and the startup funds from Clemson University (to F.D.). The simulations were performed on the Palmetto high performance cluster, which is managed and maintained by Clemson University CCIT. The authors thank Poonam Choudhary for assisting with the experiments.

Notes and references

1 G. V. Lowry, K. B. Gregory, S. C. Apte and J. R. Lead, *Environ. Sci. Technol.*, 2012, **46**, 6893–6899.
2 A. D. Maynard, R. J. Aitken, T. Butz, V. Colvin, K. Donaldson, G. Oberdorster, M. A. Philbert, J. Ryan, A. Seaton, V. Stone, S. S. Tinkle, L. Tran, N. J. Walker and D. B. Warheit, *Nature*, 2006, **444**, 267–269.
3 K. Cho, X. Wang, S. Nie, Z. G. Chen and D. M. Shin, *Clin. Cancer Res.*, 2008, **14**, 1310–1316.
4 M. E. Davis, Z. G. Chen and D. M. Shin, *Nat. Rev. Drug Discovery*, 2008, **7**, 771–782.
5 L. Zhang, F. X. Gu, J. M. Chan, A. Z. Wang, R. S. Langer and O. C. Farokhzad, *Clin. Pharmacol. Ther.*, 2008, **83**, 761–769.
6 F. Schrurs and D. Lison, *Nat. Nanotechnol.*, 2012, **7**, 546–548.
7 T. Cedervall, I. Lynch, S. Lindman, T. Berggard, E. Thulin, H. Nilsson, K. A. Dawson and S. Linse, *Proc. Natl. Acad. Sci. U. S. A.*, 2007, **104**, 2050–2055.
8 M. Lundqvist, J. Stigler, G. Elia, I. Lynch, T. Cedervall and K. A. Dawson, *Proc. Natl. Acad. Sci. U. S. A.*, 2008, **105**, 14265–14270.
9 E. Hellstrand, I. Lynch, A. Andersson, T. Drakenberg, B. Dahlback, K. A. Dawson, S. Linse and T. Cedervall, *FEBS J.*, 2009, **276**, 3372–3381.
10 A. Salvati, A. S. Pitek, M. P. Monopoli, K. Prapainop, F. B. Bombelli, D. R. Hristov, P. M. Kelly, C. Aberg, E. Mahon and K. A. Dawson, *Nat. Nanotechnol.*, 2013, **8**, 137–143.
11 A. E. Nel, L. Madler, D. Velegol, T. Xia, E. M. Hoek, P. Somasundaran, F. Klaessig, V. Castranova and M. Thompson, *Nat. Mater.*, 2009, **8**, 543–557.
12 J. Sund, H. Alenius, M. Vippola, K. Savolainen and A. Puustinen, *ACS Nano*, 2011, **5**, 4300–4309.
13 A. S. Barnard, *Nat. Nanotechnol.*, 2009, **4**, 332–335.
14 G. A. Sotiriou and S. E. Pratsinis, *Environ. Sci. Technol.*, 2010, **44**, 5649–5654.
15 C. Ge, J. Du, L. Zhao, L. Wang, Y. Liu, D. Li, Y. Yang, R. Zhou, Y. Zhao, Z. Chai and C. Chen, *Proc. Natl. Acad. Sci. U. S. A.*, 2011, **108**, 16968–16973.
16 G. Zuo, Q. Huang, G. Wei, R. Zhou and H. Fang, *ACS Nano*, 2010, **4**, 7508–7514.
17 T. A. Ratnikova, P. N. Govindan, E. Salonen and P. C. Ke, *ACS Nano*, 2011, **5**, 6306–6314.
18 J. Shang, T. A. Ratnikova, S. Anttalainen, E. Salonen, P. C. Ke and H. T. Knap, *Nanotechnology*, 2009, **20**, 415101.
19 J. W. Shen, T. Wu, Q. Wang and Y. Kang, *Biomaterials*, 2008, **29**, 3847–3855.
20 K. Kubiak and P. A. Mulheran, *J. Phys. Chem. B*, 2009, **113**, 12189–12200.
21 A. J. Makarucha, N. Todorova and I. Yarovsky, *Eur. Biophys. J.*, 2011, **40**, 103–115.
22 S. J. Marrink, A. H. de Vries and A. E. Mark, *J. Phys. Chem. B*, 2004, **108**, 750–760.

23 C. C. Chiu, G. R. Dieckmann and S. O. Nielsen, *J. Phys. Chem. B*, 2008, **112**, 16326–16333.
24 C. C. Chiu, G. R. Dieckmann and S. O. Nielsen, *Biopolymers*, 2009, **92**, 156–163.
25 A. Hung, S. Mwenifumbo, M. Mager, J. J. Kuna, F. Stellacci, I. Yarovsky and M. M. Stevens, *J. Am. Chem. Soc.*, 2011, **133**, 1438–1450.
26 S. Auer, A. Trovato and M. Vendruscolo, *PLoS Comput. Biol.*, 2009, **5**, e1000458.
27 F. Ding and N. V. Dokholyan, *Trends Biotechnol.*, 2005, **23**, 450–455.
28 F. Ding, W. Guo, N. V. Dokholyan, E. I. Shakhnovich and J. E. Shea, *J. Mol. Biol.*, 2005, **350**, 1035–1050.
29 F. Ding, Y. Furukawa, N. Nukina and N. V. Dokholyan, *J. Mol. Biol.*, 2012, **421**, 548–560.
30 D. C. Rapapport, *The art of molecular dynamics simulation*, Cambridge University Press, Cambridge, 1997.
31 F. Ding and N. V. Dokholyan, *PLoS Comput. Biol.*, 2006, **2**, e85.
32 T. Lazaridis and M. Karplus, *Curr. Opin. Struct. Biol.*, 2000, **10**, 139–145.
33 A. M. El Badawy, R. G. Silva, B. Morris, K. G. Scheckel, M. T. Suidan and T. M. Tolaymat, *Environ. Sci. Technol.*, 2010, **45**, 283–287.
34 S. Vijay-Kumar, C. E. Bugg and W. J. Cook, *J. Mol. Biol.*, 1987, **194**, 531–544.
35 G. Doni, M. A. Kostiainen, A. Danani and G. M. Pavan, *Nano Lett.*, 2011, **11**, 723–728.
36 L. Calzolai, F. Franchini, D. Gilliland and F. Rossi, *Nano Lett.*, 2010, **10**, 3101–3105.
37 F. Ding, N. V. Dokholyan, S. V. Buldyrev, H. E. Stanley and E. I. Shakhnovich, *Biophys. J.*, 2002, **83**, 3525–3532.
38 F. Ding, N. V. Dokholyan, S. V. Buldyrev, H. E. Stanley and E. I. Shakhnovich, *J. Mol. Biol.*, 2002, **324**, 851–857.
39 S. Yang, S. S. Cho, Y. Levy, M. S. Cheung, H. Levine, P. G. Wolynes and J. N. Onuchic, *Proc. Natl. Acad. Sci. U. S. A.*, 2004, **101**, 13786–13791.
40 C. Rocker, M. Potzl, F. Zhang, W. J. Parak and G. U. Nienhaus, *Nat. Nanotechnol.*, 2009, **4**, 577–580.
41 L. Vroman, *Nature*, 1962, **196**, 476–477.
42 J. N. Onuchic, P. G. Wolynes, Z. Luthey-Schulten and N. D. Socci, *Proc. Natl. Acad. Sci. U. S. A.*, 1995, **92**, 3626–3630.
43 S. Linse, C. Cabaleiro-Lago, W. F. Xue, I. Lynch, S. Lindman, E. Thulin, S. E. Radford and K. A. Dawson, *Proc. Natl. Acad. Sci. U. S. A.*, 2007, **104**, 8691–8696.

